

Article

# Method for Analyzing the Measurement Error with Respect to Azimuth and Incident Angle for the Rotating Polarizer Analyzer Ellipsometer

Huatian Tu <sup>1</sup>, Yuxiang Zheng <sup>1,\*</sup>, Yao Shan <sup>1</sup>, Yao Chen <sup>1</sup>, Haotian Zhang <sup>1</sup>, Rongjun Zhang <sup>1</sup>, Songyou Wang <sup>1</sup>, Jing Li <sup>1</sup> , YoungPak Lee <sup>1,2</sup> and Liangyao Chen <sup>1,\*</sup>

<sup>1</sup> Department of Optical Science and Engineering, Key Laboratory of Micro and Nano Photonic Structures, Ministry of Education, Shanghai Engineering Research Center of Ultra-Precision Optical Manufacturing, Fudan University, Shanghai 200433, China; 16110720002@fudan.edu.cn (H.T.); shanyao1754@163.com (Y.S.); 18210720008@fudan.edu.cn (Y.C.); 19210720003@fudan.edu.cn (H.Z.); rjzhang@fudan.edu.cn (R.Z.); sywang@fudan.ac.cn (S.W.); lijing@fudan.edu.cn (J.L.); yplee@hanyang.ac.kr (Y.L.)

<sup>2</sup> Department of Physics, Quantum Photonic Science Research Center and RINS, Hanyang University, Seoul 04763, Korea

\* Correspondence: yxzheng@fudan.edu.cn (Y.Z.); lychen@fudan.ac.cn (L.C.)

**Abstract:** We proposed a method to study the effects of azimuth and the incident angle on the accuracy and stability of rotating polarizer analyzer ellipsometer (RPAE) with bulk Au. The dielectric function was obtained at various incident angles in a range of 55°–80° and analyzed with the spectrum of the principal angle. The initial orientations of rotating polarizing elements were deviated by a series of angles to act as the azimuthal errors in various modes. The spectroscopic measurements were performed in a wavelength range of 300–800 nm with an interval of 10 nm. The repeatedly-measured ellipsometric parameters and determined dielectric constants were recorded monochromatically at wavelengths of 350, 550, and 750 nm. The mean absolute relative error was employed to evaluate quantitatively the performance of instrument. Apart from the RPAE, the experimental error analysis implemented in this work is also applicable to other rotating element ellipsometers.

**Keywords:** ellipsometry; error analysis; spectroscopy; high-accuracy measurement; optical metrology; dielectric constants



**Citation:** Tu, H.; Zheng, Y.; Shan, Y.; Chen, Y.; Zhang, H.; Zhang, R.; Wang, S.; Li, J.; Lee, Y.; Chen, L. Method for Analyzing the Measurement Error with Respect to Azimuth and Incident Angle for the Rotating Polarizer Analyzer Ellipsometer. *Crystals* **2021**, *11*, 349. <https://doi.org/10.3390/cryst11040349>

Academic Editors: Valentina Domenici and Yun-Han Lee

Received: 2 March 2021

Accepted: 25 March 2021

Published: 29 March 2021

**Publisher's Note:** MDPI stays neutral with regard to jurisdictional claims in published maps and institutional affiliations.



**Copyright:** © 2021 by the authors. Licensee MDPI, Basel, Switzerland. This article is an open access article distributed under the terms and conditions of the Creative Commons Attribution (CC BY) license (<https://creativecommons.org/licenses/by/4.0/>).

## 1. Introduction

The rotating element ellipsometer, after continuous development in many different configurations and applications, is widely employed as a primary technique in scientific research and industry [1–9]. The typical rotating element ellipsometer system comprises various types: the rotating polarizer ellipsometer (RPE) [10,11], the rotating analyzer ellipsometer (RAE) [12–14], and the rotating polarizer analyzer ellipsometer (RPAE).

The RPAE, which allows the polarizer and the analyzer to rotate in different angular velocities simultaneously, was firstly proposed by Azzam [15]. Intensive efforts have been devoted to RPAE from different aspects in past decades [16–20]. A self-established RPAE was constructed and presented in 1987 [16], with the polarizer and the analyzer rotating synchronously at an angular velocity ratio of 1:2. The system is superior in the elimination of DC signal error and phase-shift correction. Additionally, it provided two methods for the determination of ellipsometric parameters to realize the self-consistency of the data. Subsequently, the instrument was improved in 1994 [18], which enabled a fully variable incident angle by micro-stepping techniques, and employed a fixed polarizer to eliminate the effect of residual polarization from a light source.

The system and random errors have been extensively studied as an important topic in the development of ellipsometry. The accuracy and precision of ellipsometry can be

effectively improved by performing error analysis and reduction. The analyses and corrections of errors, caused by the imperfect compensator and birefringence in window, were performed by McCrackin in 1970 [21]. Aspnes systematically presented the measurement and the correction of the first-order errors [22] and the uncertainties of ellipsometric parameters [23,24]. Azzam and Bashara investigated the errors from imperfect components, cell-window birefringence, and incorrect azimuth angles [25], and performed systematic error analysis on the RAE [26]. The errors in ellipsometry have been extensively analyzed in various aspects, such as the beam deviation [27], birefringence of window [28,29], incident angle [30], azimuthal errors, and residual ellipticity [31–33]. Moreover, the systematic error analyses on different configurations have been reported, including the RAE [34], PRPSE [35], multichannel ellipsometer [36], and the Mueller matrix ellipsometer [37,38].

Although the aforementioned error analyses are conditionally applicable to the RPAE, the error investigations specifically for this type of ellipsometer are still limited. The noise effect of Fourier coefficients on the RPAE with the same configuration as in [18] was analyzed by simulation [39]. In our previous work, the systematic error reduction, induced by the analytical discrete Fourier transform, was proposed theoretically and tested experimentally [40]. Apart from the effect from the Fourier transformation, the experimental performance affected by the systematic error is worth studying further.

In this work, a method to study the error analysis on the incident angle and azimuth was presented experimentally for the self-established RPAE with bulk Au. Both spectroscopic and monochromatic repeated measurements were carried out at various incident angles. The dielectric constants were determined from the measured ellipsometric parameters to study the accuracy and stability, which were evaluated according to the differences and dispersion degrees of experimental data compared with the reference values, respectively. The initial azimuths of polarizing elements were adjusted rotationally by groups of certain angles to study the effect of azimuthal errors in three modes. The performance of RPAE was evaluated quantitatively with the mean absolute relative error (MARE). The error analysis method proposed in this work is also useful for spectroscopic ellipsometry, including temperature-dependent properties of thin polymer films and metal nanoparticles [41–44].

## 2. Materials and Methods

Figure 1 schematically illustrates the configuration of the RPAE system. A monochromator containing a rotatable grating for the wavelength scan was employed to disperse the light from the source. The monochromatic light from the exit slit passed through a collimator lens, a fixed polarizer, and a rotating polarizer in sequence before incidence on the sample. Subsequently, the reflected light went through a rotating analyzer and entered a detector for data acquisition. The acquired analog signal was converted to a digital one for data processing. The initial azimuths of polarizing elements were set along the direction perpendicular to the incident plane. The angular velocity of the rotating analyzer was controlled to be twice that of the rotating polarizer. The optical system was aligned and calibrated precisely by a low-power He-Ne laser to realize a continuously variable incident angle in a range of  $45^{\circ}$ – $90^{\circ}$ , with a computer-controlled resolution of  $0.001^{\circ}$  or a visual resolution of  $0.005^{\circ}$  [18]. The spectroscopic measurement was performed routinely through a wavelength scan in a spectral range of 300–800 nm with an interval of 10 nm. Au was selected as the test material for the low penetration depth in the visible range with a great optical stability in the atmospheric environment.

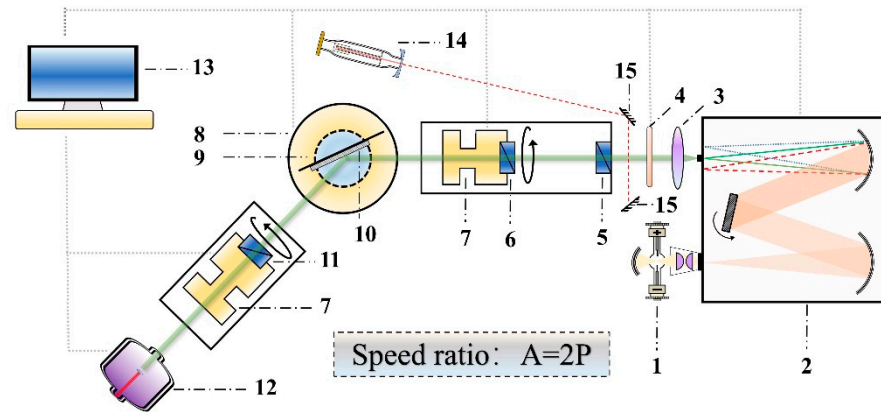


**Figure 1.** Schematic configuration of the RPAE optical system. (1) The continuous light source; (2) the monochromator consisting of two spherical mirrors and a rotatable plane grating; (3) light-collimating lens; (4) rotatable filters; (5) fixed polarizer; (6) rotating polarizer; (7) stepping motors; (8) rotating stage; (9) sample rotator; (10) sample; (11) rotating analyzer; (12) photomultiplier; (13) computer to control the monochromator, stepping motors, filters, rotating table, sample stage, and the photomultiplier; (14) laser used for alignment; and (15) mirrors to guide the laser beam for alignment.

The light intensity at the detector for RPAE is expressed as:

$$I(A) = I_0 + I_1 \cos A + I_2 \cos 2A + I_3 \cos 3A + I_4 \cos 4A, \quad (1)$$

where  $A$  represents the azimuth of analyzer and  $I_0 - I_4$  are coefficients of one direct and four harmonic components, which are obtained by applying the discrete Fourier analysis as

$$I_k = \frac{2}{n} \sum_{i=1}^n I(A_i) \cos(kA_i) \quad k = 1, 2, 3, 4, \quad (2)$$

where  $A_i$  is the  $i$ th analyzer azimuth in the measurement period. Accordingly, the ellipsometric parameters are determined by [16–18]:

$$\begin{aligned} \tan \psi_1 &= \left[ \frac{2(I_1 + I_3 - 2I_2)}{I_1 + I_3} \right]^{1/2}, \\ \cos \Delta_1 &= \frac{I_1 - 3I_3}{[2(I_1 + I_3)(I_1 + I_3 - 2I_2)]^{1/2}}, \end{aligned} \quad (3)$$

and

$$\begin{aligned} \tan \psi_2 &= \left[ \frac{9(I_1 + I_3 - 2I_2)}{2(2I_1 + I_2 + 4I_4)} \right]^{1/2}, \\ \cos \Delta_2 &= \frac{3(I_1 + I_3) - 4(I_2 + 4I_4)}{[8(I_1 + I_3)(I_1 + I_3 - 2I_2)]^{1/2}}. \end{aligned} \quad (4)$$

The two sets of solutions are self-consistent to quantitatively verify the reliability of the results without other instruments. We prefer to use Equation (3) in the experiment, since the value of  $I_4$  is the smallest in Equation (1). For bulk material measured at an incident angle of  $\theta$  in the atmosphere, the dielectric function is determined with the well-known equation:

$$\tilde{\varepsilon} = \sin^2 \theta \left[ 1 + \tan^2 \theta \left( \frac{1 - \tan \psi \cdot e^{i\Delta}}{1 + \tan \psi \cdot e^{i\Delta}} \right)^2 \right]. \quad (5)$$

The accuracy and stability are evaluated by the MARE. The value of the MARE is given by:

$$\text{MARE} = \frac{1}{n} \cdot \sum_{i=1}^n \left| \frac{x_i^{\text{measured}} - x_i^{\text{reference}}}{x_i^{\text{reference}}} \right| \times 100\%, \quad (6)$$

where  $n$  represents the amount of data.

### 3. Results

#### 3.1. Incident Angle and Principal Angle

The incident angle satisfying the condition of  $\Delta = 90^\circ$  is defined as the principal angle [45]. The error was proved theoretically to be reduced to obtain the highest precision in determining the optical constants when measured at the principal angle [17]. The spectrum of the principal angle for the Au sample was both theoretically and experimentally investigated in our previous work [46]. In this section, the ellipsometric measurements were performed by the RPAE at a series of incident angles in a range of  $55^\circ$  to  $80^\circ$ , with an interval of  $5^\circ$ , to evaluate the accuracy and stability.

##### 3.1.1. Spectroscopic Measurement

The dielectric function spectra of the Au sample at various incident angles (Figure 2) were determined from the measured ellipsometric parameters with Equation (5). The spectra showed great agreement in most of the wavelength range. On the other hand, discrepancies were observed obviously in some regions, especially in the long-wavelength range. The reference dielectric function was obtained by applying the Model dielectric function [47] and Drude model [48] to the spectra of various incident angles. Accordingly, the spectrum of the principal angle was calculated with the method presented in [46], as shown in Figure 3.

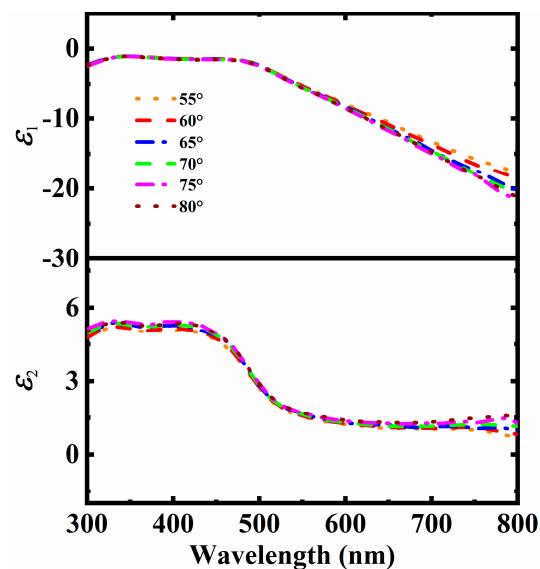


Figure 2. Dielectric functions of bulk Au determined at six incident angles.

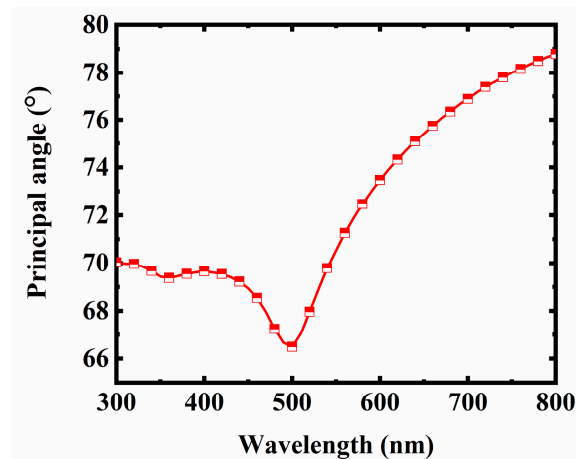


Figure 3. Spectrum of the principal angle for bulk Au.

The RPAE gave two solutions to determine the values of  $\psi$  and  $\Delta$  with Equations (3) and (4). Theoretically, the results extracted by the two solutions were expected to be equal. The differences between the two results, defined as  $\delta\psi = \psi_1 - \psi_2$  and  $\delta\Delta = \Delta_1 - \Delta_2$ , are used generally to evaluate the reliability of measurement. The values of  $\delta\psi$  and  $\delta\Delta$  in the spectral range are exhibited in Figure 4. For the incident angles in  $65^\circ$ – $80^\circ$ , the differences between the two sets varied around 0 in the spectral range, which implied good credibility for measurement. Meanwhile, the differences of  $55^\circ$  and  $60^\circ$  were relatively large, especially in the long wavelength range. As indicated in Figure 3, the principal angle increased significantly in the long wavelength range, reaching approximately  $80^\circ$ . Consequently, larger measurement errors occurred at incident angles of  $55^\circ$  and  $60^\circ$  away from the principal angle, leading to the significant discrepancy between the two solutions.

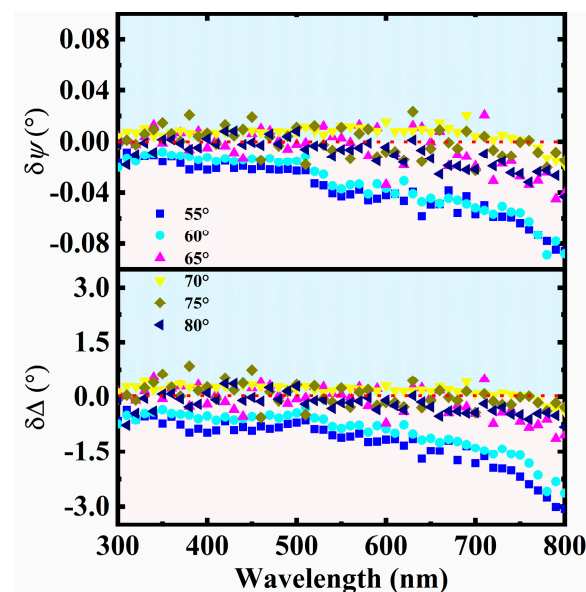


Figure 4. Discrepancies of the two sets of ellipsometric parameters at six incident angles in a spectral range.

The MARE values of the dielectric function at different incident angles are given in Table 1. The results demonstrate that the accuracy was dependent on the wavelength and corresponding principal angle. The measured results at  $65^\circ$ ,  $70^\circ$ , and  $75^\circ$  turned out to be more accurate than those measured at  $55^\circ$ ,  $60^\circ$ , and  $80^\circ$  in a wavelength range of 300–800 nm, which was consistent with the analysis based on the spectrum of the principal angle.

**Table 1.** MARE values of the dielectric functions at different incident angles.

Incident Angle (°)	55	60	65	70	75	80
MARE- $\varepsilon_1$ (%)	6.25	4.90	1.78	0.10	1.70	1.94
MARE- $\varepsilon_2$ (%)	9.12	5.45	3.8	1.39	4.19	4.19

### 3.1.2. Monochromatic Measurement

The monochromatic measurements at different incident angles were tested by performing 100 repeated measurements at a single wavelength of 350 nm. The real and imaginary parts of the reference dielectric constant at 350 nm were determined as  $\varepsilon_1 = -1.09$  and  $\varepsilon_2 = 5.2$ , respectively. The principal angle of the Au sample at 350 nm was calculated to be  $69.43^\circ$ . Figure 5a,b display the distribution of the measured ellipsometric parameters and determined dielectric constants, respectively, at six incident angles. The data amount at each incident angle in an accurate region (relative error of  $\pm 2\%$ , illustrated in Figure 5) is counted and listed in Table 2. The statistical values demonstrated that the results at  $70^\circ$ ,  $65^\circ$ , and  $75^\circ$  had more accurate data compared with the others, which was consistent with the theoretical analysis of the principal angle.

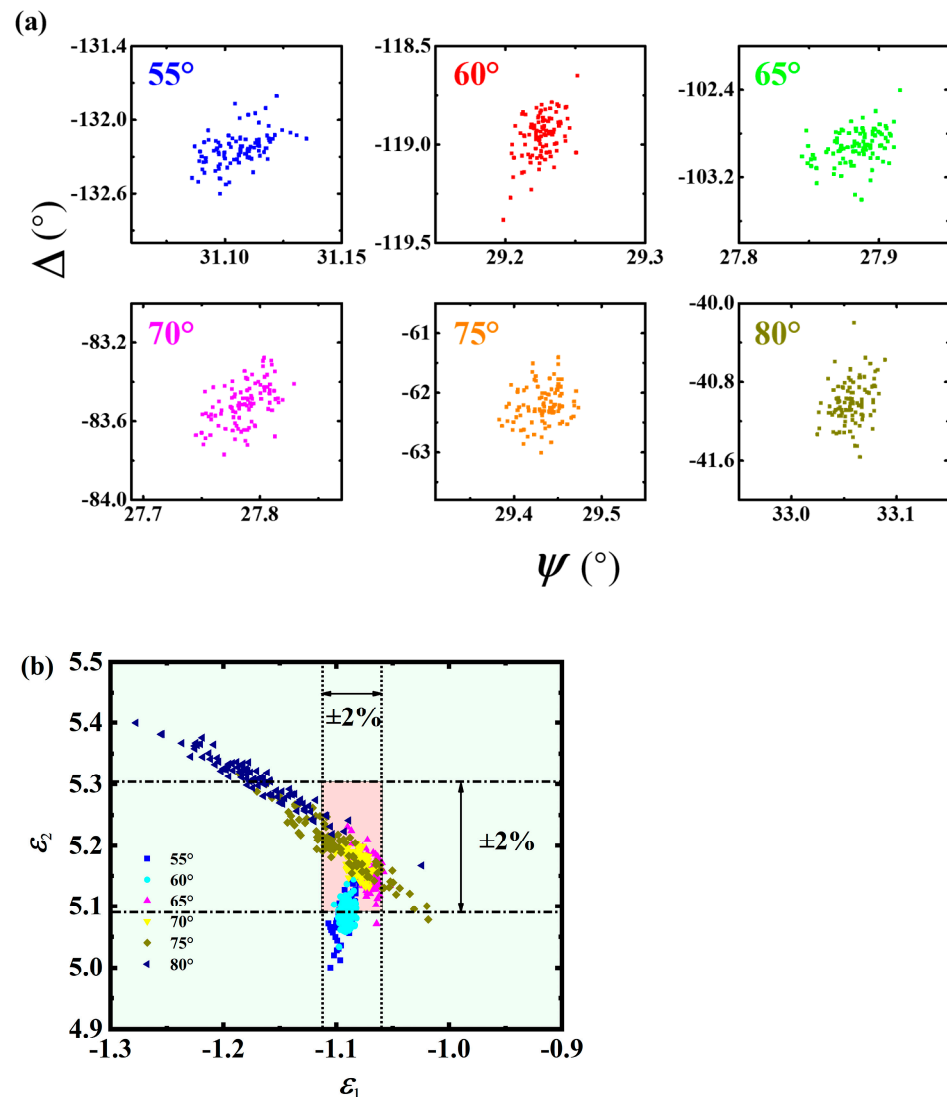


**Figure 5.** Distribution of the 100 (a) repeatedly-measured ellipsometric parameters, and (b) determined dielectric constants for six incident angles at a wavelength of 350 nm.

**Table 2.** Amounts of data points in an accurate region shown in Figure 5 in the 100 repeated measurements for different incident angles at a wavelength of 350 nm.

Incident Angle (°)	55	60	65	70	75	80
Amount of data points	30	27	96	100	68	8

The repeated measurement procedure was performed subsequently on two other wavelengths of 550 and 750 nm at different incident angles. The corresponding MAREs of the real part of the dielectric constant with varying incident angles were calculated at three wavelength points, as indicated in Figure 6. The principal angles of the Au sample at 350, 550, and 750 nm were determined to be 69.43°, 70.53°, and 78.01°, respectively. The MARE versus incident angle implies that the measurement exhibited higher accuracy and smaller error with the incident angle close to the principal angle. For example, the MARE at 750 nm decreased significantly with the increasing incident angle, which was attributed to the corresponding principal angle of 78.01°. At incident angles of 65°, 70°, and 75°, the MAREs turned out to be relatively small at all three wavelengths in Figure 6, representing the short, middle, and long wavelength parts in the spectral range. Accordingly, the results indicated that these three incident angles enabled accurate measurement for the Au sample and some other typical metals.

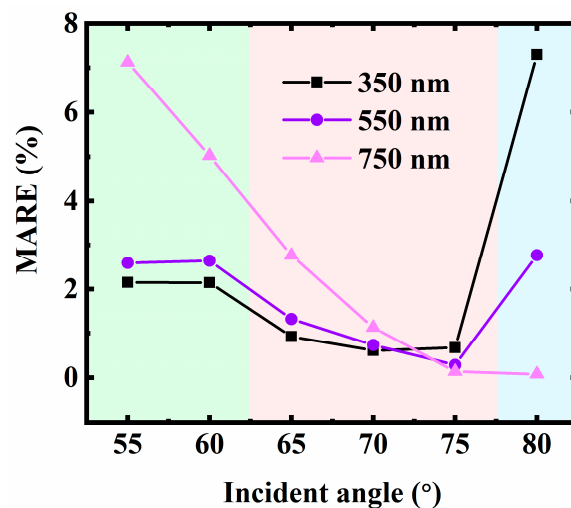


**Figure 6.** Values of MARE versus the incident angle at three wavelengths.

### 3.2. Azimuthal Error

In the rotating element ellipsometers, the measurement is fundamentally based on the detection of different polarization states, which is usually realized with the rotating elements. Consequently, the azimuthal error of the polarizing element significantly affects the performance of the instrument. In this subsection, we experimentally investigated the effect of the azimuthal error on the accuracy and stability of the results. The initial azimuths of the polarizer and analyzer were adjusted rotationally by a certain angle from the s-axis to act as the azimuthal errors, represented as  $\delta\theta_P$  and  $\delta\theta_A$ , respectively.

#### 3.2.1. Theoretical Analysis

For the measurement with the azimuthal error  $\delta$ , assuming that the condition  $A = 2P$  is still satisfied, the expression of light intensity in Equation (1) is modified as:

$$I_{\delta}(A) = I_0 + I_1 \cos(A + \delta) + I_2 \cos 2(A + \delta) + I_3 \cos 3(A + \delta) + I_4 \cos 4(A + \delta). \quad (7)$$

Compared with Equation (2), the four harmonic components are determined as:

$$I_{k\delta} = \frac{2}{\cos k\delta \cdot n} \sum_{i=1}^n I_{\delta}(A_i) \cos(kA_i) = \sec k\delta \cdot I_k \quad k = 1, 2, 3, 4. \quad (8)$$

Consequently, the ellipsometric parameters obtained in experiment are given as:

$$\begin{aligned} \tan \psi_{\delta 1} &= \left[ \frac{2(I_1 \cdot \sec \delta + I_3 \cdot \sec 3\delta - 2I_2 \cdot \sec 2\delta)}{I_1 \cdot \sec \delta + I_3 \cdot \sec 3\delta} \right]^{1/2}, \\ \cos \Delta_{\delta 1} &= \frac{I_1 \cdot \sec \delta - 3I_3 \cdot \sec 3\delta}{[2(I_1 \cdot \sec \delta + I_3 \cdot \sec 3\delta)(I_1 \cdot \sec \delta + I_3 \cdot \sec 3\delta - 2I_2 \cdot \sec 2\delta)]^{1/2}}, \end{aligned} \quad (9)$$

and

$$\begin{aligned} \tan \psi_{\delta 2} &= \left[ \frac{9(I_1 \cdot \sec \delta + I_3 \cdot \sec 3\delta - 2I_2 \cdot \sec 2\delta)}{2(2I_1 \cdot \sec \delta + I_2 \cdot \sec 2\delta + 4I_4 \cdot \sec 4\delta)} \right]^{1/2}, \\ \cos \Delta_{\delta 2} &= \frac{3(I_1 \cdot \sec \delta + I_3 \cdot \sec 3\delta) - 4(I_2 \cdot \sec 2\delta + 4I_4 \cdot \sec 4\delta)}{[8(I_1 \cdot \sec \delta + I_3 \cdot \sec 3\delta)(I_1 \cdot \sec \delta + I_3 \cdot \sec 3\delta - 2I_2 \cdot \sec 2\delta)]^{1/2}}. \end{aligned} \quad (10)$$

### 3.2.2. Experimental Results

Firstly, the ellipsometric parameters of the Au sample were measured by the RPAE at an incident angle of  $70^\circ$  in a wavelength range of 300–800 nm, with  $\delta\theta_P$  varying from 0– $20^\circ$ , as shown in Figure 7a. The spectra of  $\psi$  and  $\Delta$  demonstrated that the measured results deviated significantly from the standard spectra with the increasing of the azimuthal error of the polarizer. Similarly, the ellipsometric measurements were performed with  $\delta\theta_A$  varying from 0– $20^\circ$ , as shown in Figure 7b. The spectra of  $\psi$  deviated differently compared with those of  $\delta\theta_P$ . Since the analyzer and polarizer rotated at an angular velocity ratio of 1:2 in measurement, the values of  $\delta\theta_A$  and  $\delta\theta_P$  were set at a group of angles with the same ratio. The value of  $\delta\theta_A$  varied from 0– $20^\circ$ , compared with that of  $\delta\theta_P$  in a range of 0– $10^\circ$ . Hence, the azimuth of the analyzer was always twice that of the polarizer during rotation. The same procedure was repeated to get the spectra of  $\psi$  and  $\Delta$  (Figure 7c).

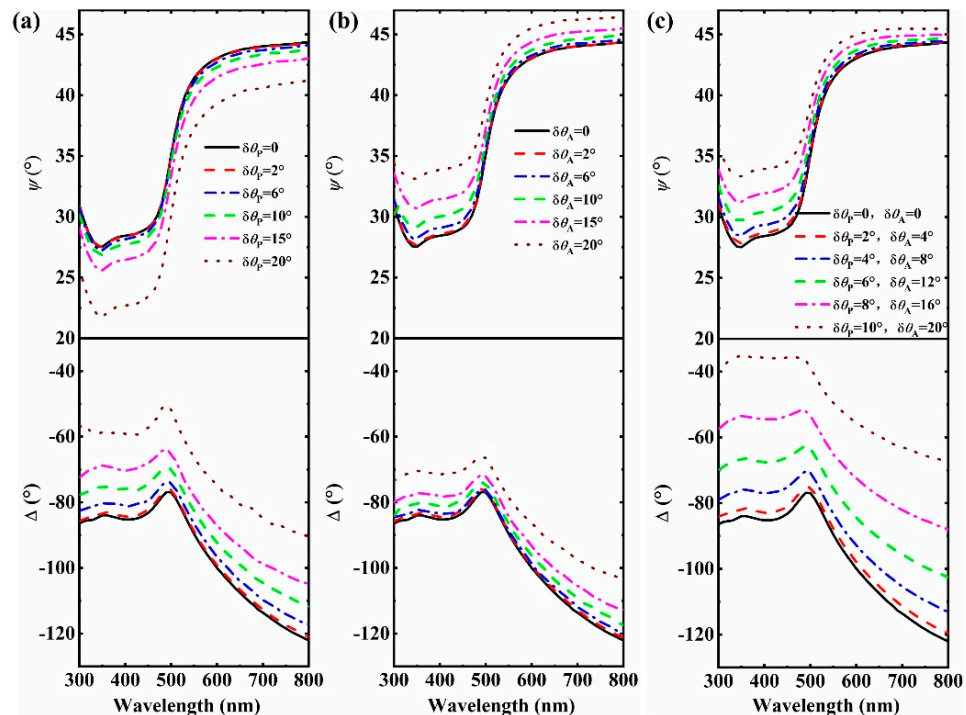
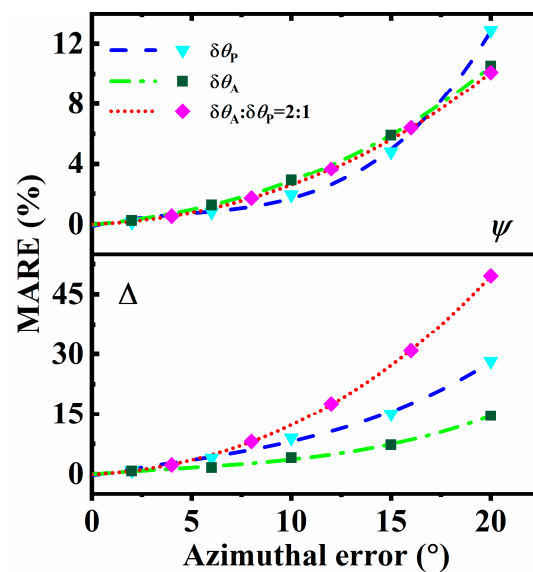


Figure 7. Measured ellipsometric parameters with various azimuthal errors of (a) the polarizer, (b) analyzer, and (c) both at a ratio of 1:2.

The MAREs of  $\psi$  and  $\Delta$  were calculated and fitted into curves by applying the polynomial fitting method for three azimuthal error modes, as displayed in Figure 8. The comparison revealed the effect of the azimuthal error on the accuracy quantitatively. For the MARE of  $\psi$ , the three curves behaved similarly with small azimuthal errors, while the value increased significantly with a large value of  $\delta\theta_P$ . As for  $\Delta$ , the value increased slightly for the curve of  $\delta\theta_A$ , while rapidly for that of  $\delta\theta_P$  and  $\delta\theta_P:\delta\theta_A = 1:2$ . Therefore, the azimuthal error of the polarizer was indicated to more seriously affect the accuracy of the RPAE.

The polarizing elements were rotated in the opposite direction with the same absolute values of azimuthal errors to study the directional dependence on accuracy. The spectra of  $\psi$  and  $\Delta$ , measured for a series of the same absolute values, showed a high consistency for both  $\pm\delta\theta_P$  and  $\pm\delta\theta_A$ , as observed in Figure 9. Consequently, the accuracy of the RPAE was found to be less dependent on the direction of the azimuthal error in terms of the acquired spectra.



**Figure 8.** Experimental data (points) and fitted curves (lines) of MAREs versus azimuthal errors (for  $\delta\theta_A:\delta\theta_P = 2:1$ , the horizontal axis represents  $\delta\theta_A$ ).

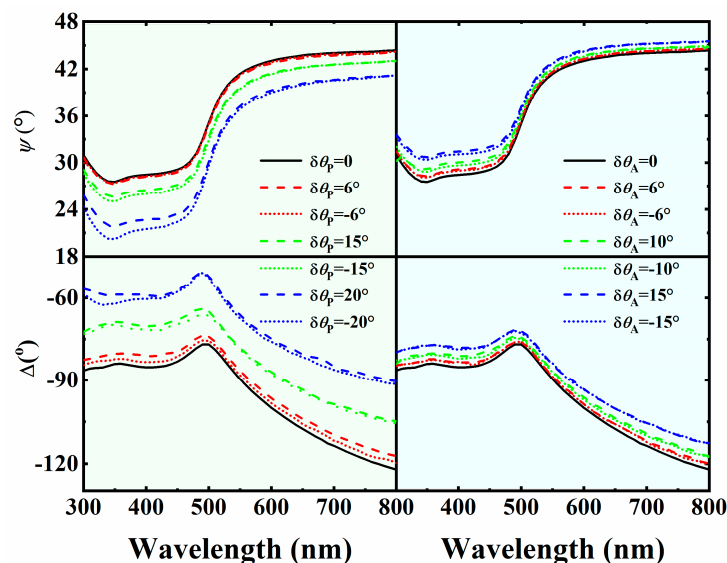


**Figure 9.** Ellipsometric parameters measured with azimuthal errors of the same absolute values in the opposite direction.

#### 4. Conclusions

We presented a method to implement the experimental error analysis of azimuth and the incident angle specifically for the RPAE in this work. The dielectric functions of bulk Au were determined from the measured  $\psi$  and  $\Delta$  at incident angles in a range of  $55^\circ$ – $80^\circ$ , with an interval of  $5^\circ$ , to study the effect on the instrument. The results acquired at an incident angle close to the principal angle were observed to exhibit higher accuracy and better stability, according to the discrepancies between the two solutions, and the values of the MARE. The azimuthal error analysis was performed experimentally with the initial orientations of polarizing elements deviating from the zero azimuth. The fitting curves of the MARE versus azimuthal error suggest that  $\delta\theta_P$  more seriously affects the accuracy of the RPAE. The demonstrated error analysis reveals the relationship between the acquired data and experimental conditions, which gives access to achieving accurate and reliable measurement by using the RPAE, and is easily generalized to other rotating element ellipsometers.

**Author Contributions:** Conceptualization, H.T. and Y.Z.; methodology, H.T.; validation, Y.S., Y.C., and H.Z.; formal analysis, H.T. and Y.S.; investigation, Y.C. and H.Z.; data curation, Y.Z., Y.L. and L.C.; writing—original draft preparation, H.T.; writing—review and editing, Y.Z., R.Z., S.W., J.L., Y.L. and L.C.; supervision, Y.Z. and L.C.; project administration, Y.Z. and L.C.; funding acquisition, Y.Z. and L.C. All authors have read and agreed to the published version of the manuscript.

**Funding:** This research was funded by the National Natural Science Foundation of China, grant number 61775042 11674062 and the Fudan University CIOMP Joint Fund, grant number FC2017-003.

**Institutional Review Board Statement:** Not applicable.

**Informed Consent Statement:** Not applicable.

**Data Availability Statement:** Not applicable.

**Acknowledgments:** We would like to express our sincere appreciations to the anonymous referees for valuable suggestions and corrections.

**Conflicts of Interest:** The authors declare no conflict of interest.

#### References

1. Azzam, R.M.A.; Bashara, N.M. *Ellipsometry and Polarized Light*; North-Holland: Amsterdam, The Netherlands, 1977.
2. Hauge, P.S. Recent developments in instrumentation in ellipsometry. *Surf. Sci.* **1980**, *96*, 108–140. [[CrossRef](#)]
3. Woollam, J.A.; Snyder, P.G.; Rost, M.C. Variable angle spectroscopic ellipsometry—A non-destructive characterization technique for ultrathin and multilayer materials. *Thin Solid Film.* **1988**, *166*, 317–323. [[CrossRef](#)]
4. Collins, R.W. Automatic rotating element ellipsometers: Calibration, operation, and real-time applications. *Rev. Sci. Instrum.* **1990**, *61*, 2029–2062. [[CrossRef](#)]
5. Aspnes, D.E. Expanding horizons: New developments in ellipsometry and polarimetry. *Thin Solid Film.* **2004**, *455–456*, 3–13. [[CrossRef](#)]
6. Tompkins, H.G.; Irene, E.A. *Handbook of Ellipsometry*; William Andrew: New York, NY, USA, 2005.
7. Fujiwara, H. *Spectroscopic Ellipsometry: Principles and Applications*; John Wiley & Sons: Tokyo, Japan, 2007.
8. Aspnes, D.E. Spectroscopic ellipsometry—Past, present, and future. *Thin Solid Film.* **2014**, *571*, 334–344. [[CrossRef](#)]
9. Azzam, R.M.A. Polarization, thin-film optics, ellipsometry, and polarimetry: Retrospective. *J. Vac. Sci. Technol. B* **2019**, *37*, 060802. [[CrossRef](#)]
10. Cahan, B.D.; Spanier, R.F. A high speed precision automatic ellipsometer. *Surf. Sci.* **1969**, *16*, 166–176. [[CrossRef](#)]
11. Stobie, R.W.; Rao, B.; Dignam, M.J. Analysis of a novel ellipsometric technique with special advantages for infrared spectroscopy. *J. Opt. Soc. Am.* **1975**, *65*, 25–28. [[CrossRef](#)]
12. Aspnes, D.E. Fourier transform detection system for rotating-analyzer ellipsometers. *Opt. Commun.* **1973**, *8*, 222–225. [[CrossRef](#)]
13. Aspnes, D.E.; Studna, A.A. High Precision Scanning Ellipsometer. *Appl. Opt.* **1975**, *14*, 220. [[CrossRef](#)]
14. Schubert, M.; Rheinlander, B.; Woollam, J.A.; Johs, B.; Herzinger, C.M. Extension of rotating-analyzer ellipsometry to generalized ellipsometry: Determination of the dielectric function tensor from uniaxial  $\text{TiO}_2$ . *J. Opt. Soc. Am.* **1996**, *13*, 875. [[CrossRef](#)]
15. Azzam, R.M.A. A simple Fourier photopolarimeter with rotating polarizer and analyzer for measuring Jones and Mueller matrices. *Opt. Commun.* **1978**, *25*, 137–140. [[CrossRef](#)]
16. Chen, L.Y.; Lynch, D.W. Scanning ellipsometer by rotating polarizer and analyzer. *Appl. Opt.* **1987**, *26*, 5221–5228. [[CrossRef](#)]

17. Chen, L.Y.; Feng, X.W.; Su, Y.; Ma, H.Z.; Qian, Y.H. Improved rotating analyzer-polarizer type of scanning ellipsometer. *Thin Solid Films* **1993**, *234*, 385–389. [[CrossRef](#)]
18. Chen, L.Y.; Feng, X.W.; Su, Y.; Ma, H.Z.; Qian, Y.H. Design of a scanning ellipsometer by synchronous rotation of the polarizer and analyzer. *Appl. Opt.* **1994**, *33*, 1299–1305. [[CrossRef](#)]
19. El-Agez, T.M.; El Tayyan, A.A.; Taya, S.A. Rotating polarizer-analyzer scanning ellipsometer. *Thin Solid Film.* **2010**, *518*, 5610–5614. [[CrossRef](#)]
20. El-Agez, T.M.; Taya, S.A. Development and construction of rotating polarizer analyzer ellipsometer. *Opt. Laser. Eng.* **2011**, *49*, 507–513. [[CrossRef](#)]
21. Mccrackin, F.L. Analyses and corrections of instrumental errors in ellipsometry. *J. Opt. Soc. Am.* **1970**, *60*, 57–63. [[CrossRef](#)]
22. Aspnes, D.E. Measurement and correction of first-order errors in ellipsometry. *J. Opt. Soc. Am.* **1971**, *61*, 1077–1085. [[CrossRef](#)]
23. Aspnes, D.E. Optimizing precision of rotating-analyzer ellipsometers. *J. Opt. Soc. Am.* **1974**, *64*, 639–646. [[CrossRef](#)]
24. Aspnes, D.E. Optimizing precision of rotating-analyzer and rotating-compensator-ellipsometers. *J. Opt. Soc. Am.* **2004**, *21*, 403–410. [[CrossRef](#)] [[PubMed](#)]
25. Azzam, R.M.A.; Bashara, N.M. Unified analysis of ellipsometry errors due to imperfect components, cell-window birefringence, and incorrect azimuth angles. *J. Opt. Soc. Am.* **1971**, *61*, 600–607. [[CrossRef](#)]
26. Azzam, R.M.A.; Bashara, N.M. Analysis of systematic errors in rotating-analyzer ellipsometers. *J. Opt. Soc. Am.* **1974**, *64*, 1459–1469. [[CrossRef](#)]
27. Zeidler, J.R.; Kohles, R.B.; Bashara, N.M. Beam Deviation Errors in Ellipsometric Measurements; an Analysis. *Appl. Opt.* **1974**, *13*, 1938–1945. [[CrossRef](#)]
28. Jin, L.; Kasuga, S.; Kondoh, E. General window correction method for ellipsometry measurements. *Opt. Express* **2014**, *22*, 27811–27820. [[CrossRef](#)]
29. Nissim, N.; Eliezer, S.; Bakshi, L.; Moreno, D.; Perelmutter, L. In situ correction of windows' linear birefringence in ellipsometry measurements. *Opt. Commun.* **2009**, *282*, 3414–3420. [[CrossRef](#)]
30. Humlicek, J. Sensitivity extrema in multiple-angle ellipsometry. *J. Opt. Soc. Am. A* **1985**, *2*, 713–722.31. [[CrossRef](#)]
31. Kleim, R.; Kuntzler, L.; El Ghemmaz, A. Systematic errors in rotating-compensator ellipsometry. *J. Opt. Soc. Am. A* **1994**, *11*, 2550–2559. [[CrossRef](#)]
32. Bertucci, S.; Pawlowski, A.; Nicolas, N.; Johann, L.; El Ghemmaz, A.; Stein, N.; Kleim, R. Systematic errors in fixed polarizer, rotating polarizer, sample, fixed analyzer spectroscopic ellipsometry. *Thin Solid Films* **1998**, *313–314*, 73–78. [[CrossRef](#)]
33. Chao, Y.F.; Lee, K.Y.; Lin, Y.D. Analytical solutions of the azimuthal deviation of a polarizer and an analyzer by polarizer-sample-analyzer ellipsometry. *Appl. Opt.* **2006**, *45*, 3935–3939. [[CrossRef](#)]
34. Nijs, J.M.M.; Silfhout, A.V. Systematic and random errors in rotating-analyzer, ellipsometry. *J. Opt. Soc. Am. A* **1988**, *5*, 773–781. [[CrossRef](#)]
35. En Naciri, A.; Broch, L.; Johann, L.; Kleim, R. Fixed polarizer, rotating-polarizer and fixed analyzer spectroscopic ellipsometer: Accurate calibration method, effect of errors and testing. *Thin Solid Films* **2002**, *406*, 103–112. [[CrossRef](#)]
36. Nguyen, N.V.; Pudliner, B.S.; An, I.; Collins, R.W. Error correction for calibration and data reduction in rotating-polarizer ellipsometry applications to a novel multichannel ellipsometer. *J. Opt. Soc. Am. A* **1991**, *8*, 919–931. [[CrossRef](#)]
37. Nee, S. Error analysis for Mueller matrix measurement. *J. Opt. Soc. Am. A* **2003**, *20*, 1651–1657. [[CrossRef](#)]
38. Broch, L.; Naciri, A.E.; Johann, L. Systematic errors for a Mueller matrix dual rotating compensator ellipsometer. *Opt. Express* **2008**, *16*, 8814–8824. [[CrossRef](#)] [[PubMed](#)]
39. El-Agez, T.M.; Taya, S.A. An extensive theoretical analysis of the 1:2 ratio rotating polarizer-analyzer Fourier ellipsometer. *Phys. Scr.* **2011**, *83*, 25701. [[CrossRef](#)]
40. Mao, P.; Zheng, Y.; Cai, Q.; Zhang, D.; Zhang, R.; Zhao, H.; Chen, L. Approach to Error Analysis and Reduction for Rotating-Polarizer-Analyzer Ellipsometer. *J. Phys. Soc. Jpn.* **2012**, *81*, 124003. [[CrossRef](#)]
41. Hajduk, B.; Bednarski, H.; Trzebicka, B. Temperature-Dependent Spectroscopic Ellipsometry of Thin Polymer Films. *J. Phys. Chem. B* **2020**, *124*, 3229–3251. [[CrossRef](#)] [[PubMed](#)]
42. Nosidlak, N.; Jaglarz, J.; Danel, A. Ellipsometric studies for thin polymer layers of organic photovoltaic cells. *J. Vac. Sci. Technol. B* **2019**, *37*, 062402. [[CrossRef](#)]
43. Hajduk, B.; Bednarski, H.; Jarzabek, B.; Nitschke, P.; Janeczek, H. Phase diagram of P3HT:PC70BM thin films based on variable-temperature spectroscopic ellipsometry. *Polym. Test* **2020**, *84*, 106383. [[CrossRef](#)]
44. Jarzabek, B.; Nitschke, P.; Hajduk, B.; Domański, M.; Bednarski, H. In situ thermo-optical studies of polymer:fullerene blend films. *Polym. Test* **2020**, *88*, 106573. [[CrossRef](#)]
45. Azzam, R.M.A. Contours of constant principal angle and constant principal azimuth in the complex epsilon-plane. *J. Opt. Soc. Am. A* **1981**, *71*, 1523–1528. [[CrossRef](#)]
46. Zhu, X.; Zhao, H.; Zhang, R.; Ma, Y.; Liu, Z.; Li, J.; Shen, Z.; Wang, S.; Chen, L. Analytical study of the principal angle used in optical experiments. *Appl. Opt.* **2002**, *41*, 2592–2595. [[CrossRef](#)] [[PubMed](#)]
47. Aspnes, D.E.; Kinsbron, E.; Bacon, D.D. Optical-properties of Au: Sample effects. *Phys. Rev. B* **1980**, *21*, 3290–3299. [[CrossRef](#)]
48. Takeuchi, K.; Adachi, S. Optical properties of  $\beta$ -Sn films. *J. Appl. Phys.* **2009**, *105*, 073520. [[CrossRef](#)]